NeuroImage 195 (2019) 243–251

Contents lists available at ScienceDirect

NeuroImage

journal homepage: www.elsevier.com/locate/neuroimage

Abnormal axon guidance signals and reduced interhemispheric connection via anterior commissure in neonates of marmoset ASD model

Koki Mimura [a,b], Tomofumi Oga [a], Tetsuya Sasaki [a,h], Keiko Nakagaki [a], Chika Sato [c], Kayo Sumida [d], Kohei Hoshino [e], Koichi Saito [d], Izuru Miyawaki [e], Tetsuya Suhara [b], Ichio Aoki [c,f], Takafumi Minamimoto [b,*], Noritaka Ichinohe [a,g,**]

[a] Department of Ultrastructural Research, National Institute of Neuroscience, National Center of Neurology and Psychiatry, 4-1-1 Ogawa-Higashi, Kodaira, Tokyo, 187-8502, Japan
[b] Department of Functional Brain Imaging, National Institute of Radiological Sciences, National Institutes for Quantum and Radiological Science and Technology (QST), 4-9-1 Anagawa, Inage-ku, Chiba, Chiba, 263-8555, Japan
[c] Department of Molecular Imaging and Theranostics, National Institute of Radiological Sciences, QST, Anagawa 4-9-1, Inage, Chiba, 263-8555, Japan
[d] Environmental Health Science Laboratory, Sumitomo Chemical Co., Ltd., 3-1-98 Kasugade-naka, Konohana-ku, Osaka, 554-8558, Japan
[e] Preclinical Research Laboratories, Dainippon Sumitomo Pharma Co., Ltd., 3-1-98 Kasugade-naka, Konohana-ku, Osaka, 554-0022, Japan
[f] Group of Quantum-state Controlled MRI, QST, Anagawa 4-9-1, Inage, Chiba, 263-8555, Japan
[g] Ichinohe Group, Laboratory for Molecular Analysis of Higher Brain Function, RIKEN Brain Science Institute, 2-1 Hirosawa, Wako, Saitama, 351-0198, Japan
[h] Department of Anatomy and Neuroscience, Faculty of Medicine, University of Tsukuba, Tsukuba, Ibaraki, 305-8577, Japan

ARTICLE INFO

Keywords:
MRI
Monkey
Axon guidance
DTI
Social brain
Interhemispheric connection

ABSTRACT

In autism spectrum disorder (ASD), disrupted functional and structural connectivity in the social brain has been suggested as the core biological mechanism underlying the social recognition deficits of this neurodevelopmental disorder. In this study, we aimed to identify genetic and neurostructural abnormalities at birth in a non-human primate model of ASD, the common marmoset with maternal exposure to valproic acid (VPA), which has been reported to display social recognition deficit in adulthood. Using a comprehensive gene expression analysis, we found that 20 genes were significantly downregulated in VPA-exposed neonates. Of these, *Frizzled3* (*FZD3*) and *PIK3CA* were identified in an axon guidance signaling pathway. *FZD3* is essential for the normal development of the anterior commissure (AC) and corpus callosum (CC); hence, we performed diffusion tensor magnetic resonance imaging with a 7-Tesla scanner to measure the midsagittal sizes of these structures. We found that the AC size in VPA-exposed neonates was significantly smaller than that in age-matched controls, while the CC size did not differ. These results suggest that downregulation of the genes related to axon guidance and decreased AC size in neonatal primates may be linked to social brain dysfunctions that can happen later in life.

1. Introduction

Autism spectrum disorder (ASD) is one of the most common neurodevelopmental disorders involving social communication and interaction disabilities, and particularly an inability to mentalize and infer another person's state of mind (Frith et al., 1991). Social perception (i.e., mentalizing or "Theory of Mind") is thought to be processed in a set of interconnected neuroanatomical structures such as the orbitofrontal cortex (OFC), posterior superior temporal sulcus, inferior temporal cortex, and amygdala — termed the 'social brain' (Hervé et al., 2012; Ross et al., 2010; Gallagher et al., 2003). Numerous neuroimaging studies on ASD patients have reported disrupted structural and functional connectivity in their social brain (Wass et al., 2011; Pelphrey et al., 2011; Di Martino et al., 2009; Wicker et al., 2008). ASD is an early-onset

Abbreviations: AC, anterior commissure; ASD, autism spectrum disorder; CC, corpus callosum; FC, fold change; *FZD3*, *Frizzled3*; DTI, diffusion tensor imaging; PFC, prefrontal cortex; WB, whole brain.

* Corresponding author. Department of Functional Brain Imaging, National Institute of Radiological Sciences, National Institutes for Quantum and Radiological Science and Technology, 4-9-1, Anagawa, Inage-ku, Chiba, 263-8555, Japan.
** Corresponding author. Department of Ultrastructural Research, National Institute of Neuroscience, National Center of Neurology and Psychiatry, 4-1-1 Ogawa-Higashi, Kodaira, Tokyo, 187-8502, Japan.
E-mail addresses: minamimoto.takafumi@qst.go.jp (T. Minamimoto), nichinohe@ncnp.go.jp (N. Ichinohe).

https://doi.org/10.1016/j.neuroimage.2019.04.006
Received 12 October 2018; Received in revised form 18 March 2019; Accepted 2 April 2019
Available online 3 April 2019

neurodevelopmental disorder that occurs within the first 3 years of life; therefore, it is important to understand the genetic and neurostructural risks for neonatal development of the social brain in order to provide an opportunity for effective early intervention (~12–48 months) (Vivanti et al., 2016; Robins et al., 2008). Recent studies have suggested that ASD or ASD-high-risk children aged 6–12 months already present an atypical neurostructural phenotype, especially in their interhemispheric connections (Hazlett et al., 2017; Wolff et al., 2015). However, apparent technical limitations in human studies have prevented the identification of causal genetic and/or neurostructural factors for atypical social brain development.

Non-human primates have strong similarities to humans in terms of brain structure and social communication abilities, and hence are considered a good model for studying social brain dysfunction (Nelson and Winslow, 2009; Zhao et al., 2018). Especially, the common marmoset (*Callithrix jacchus*), which exhibits human-like social cognitive abilities, has become a popular primate model for studying biological foundations of human social cognition (Burkart et al., 2007; Yamazaki and Watanabe, 2009). For example, the marmoset distinguishes human actors who reciprocate social exchanges from those who do not, so that it refuses food from non-reciprocators (Kawai et al., 2014). The animal is also sensitive and averse to reward inequality (Yasue et al., 2018). These human-like social behaviors were impaired in the ASD model marmoset with prenatal exposure to the anti-epilepsy drug valproic acid (VPA) (Yasue et al., 2015, 2018), which is known to increase the risk of ASD in humans (Christensen et al., 2013). Such a higher-order and complex nature of social recognition deficits is remarkable among various social deficits (e.g., less social interaction) displayed in other ASD animal models; therefore, studying a neonatal marmoset VPA model may provide a good opportunity to reveal the genetic and neurostructural differences underlying atypical social brain development.

In this study, we aimed to identify, at birth, the genetic and neurostructural signatures in the marmoset that underlie social recognition impairment in later life. We performed comprehensive gene expression analysis of the social brain to identify VPA-associated abnormalities in neonatal marmosets in comparison with age-matched controls. The results showed significant downregulation of gene expression in VPA-exposed neonates, including *Frizzled3* (*FZD3*) and *PIK3CA*, both of which are on the axon guidance signaling pathway. *FZD3* is essential for normal embryonic development of the anterior commissure (AC) and corpus callosum (CC) — bundles of axons connecting the two brain hemispheres, including the social brain (Wang et al., 2002, 2006; Hua et al., 2014). Thus, we examined structural abnormalities in AC and CC of VPA-exposed neonates using diffusion tensor imaging (DTI). We found that the midsagittal AC size in VPA-exposed neonates was significantly smaller than that in age-matched controls, while there was no difference in CC size. The findings of this study may provide novel genetic and neurostructural signatures at birth that underlie autism-associated behaviors in primates, and could be potential targets for early intervention of ASD.

2. Materials and methods

2.1. Subjects and experimental design

In this study, we used 24 neonatal common marmosets [postnatal day (P)0–P4; Table 1]; 11 of these were exposed to VPA *in utero* (VPA group), while the remaining 13 were unexposed (UE/control group). Eight neonatal marmosets (VPA: $n = 4$; UE: $n = 4$) were used for microarray gene expression analysis, while 16 (VPA: $n = 7$; UE: $n = 9$) were used for magnetic resonance imaging (MRI) measurements (Table 1). The microarray data from the UE group had also been used in previous studies (Sasaki et al., 2014a, 2014b). Marmosets and their dams were housed in a family cage and were provided food (CMS-1, CREA-Japan Inc., Tokyo, Japan) and water ad libitum. The family cage was exposed to a 12-h light–dark cycle. The room temperature and humidity were maintained at ~27°C–30 °C and ~40%–50%, respectively.

All experimental and animal care procedures were approved by the Animal Research Committee, National Center of Neurology and Psychiatry (NCNP), Tokyo, Japan, and the National Institute of Radiological Sciences, Chiba, Japan, and were in accordance with the US National Institutes of Health *Guide for the Care and Use of Laboratory Animals* (NIH Publication No. 80–23) and the *Guide for Care and Use of Laboratory Primates* published by the National Institute of Neuroscience, NCNP.

VPA marmosets were obtained using the same procedure as previously described (Yasue et al., 2015, 2018). Briefly, the dams were mated in their pair cages, and their blood progesterone levels were periodically monitored to determine the timing of pregnancy. Blood samples (<0.3 mL) were collected twice a week from the femoral vein of unanesthetized animals put in a restrainer (CL-4532, CLEA, Japan, Inc.). The dams received seven oral administrations of VPA sodium salt (200 mg/kg/day; Sigma-Aldrich, St. Louis, Mo) from days 60 through 66 after conception (Fig. 1). VPA was dissolved in 10% glucose solution just prior to administration.

2.2. Microarray analysis

Marmosets ($n = 8$; Table 1) were sedated with 25 mg/kg ketamine hydrochloride (Ketalar®, Daiichi Sankyo, Tokyo, Japan) administered intramuscularly and then euthanized using an overdose of 100 mg/kg sodium pentobarbital (Somnopentyl®, BCM International, Hillsborough, NJ, USA) administered intraperitoneally. Next, they were intracardially perfused with 0.1 M potassium phosphate-buffered saline (PBS; pH 7.2). Tissue blocks from OFC (mainly area 12) (Burman and Rosa, 2009) and the temporal association cortex (mainly area TE) were excised as previously described (Oga et al., 2013), and immersed in RNA later (Life Technologies Japan Ltd., Tokyo, Japan). Total RNA samples were prepared using the RNeasy Mini Kit (Qiagen, Valencia, CA, USA) according to the manufacturer's instructions. The RNA concentrations were measured using a NanoDrop 2000 spectrophotometer (Thermo Fisher Scientific, Wilmington, DE, USA), and RNA integrity was assessed using a 2100 Bioanalyzer (Agilent, Santa Clara, CA, USA; RNA integrity number >7.0). Microarray probing, reverse transcription, second-strand synthesis, and probe generation were performed using the 30IVT Express Kit (Affymetrix, Santa Clara, CA, USA) according to the manufacturer's instructions. In brief, double-stranded cDNA was synthesized using 100 ng of total RNA. This cDNA was then used to prepare biotin-labeled cRNA. Finally, 15 μg of labeled cRNA was fragmented.

Next, gene expression was quantified using custom-made microarrays (Marmo2a520631 F) (Sasaki et al., 2014a, 2014b). The microarrays were hybridized according to instructions given in the *Gene Chip Expression Analysis Technical Manual* (Affymetrix). The microarrays were stained and washed using the GeneChip Hybridization, Wash, and Stain Kit (Affymetrix). Fluorescence was intensified using the antibody amplification method according to the manufacturer's instructions. The microarrays were then scanned with a GeneChip Scanner 3000 (Affymetrix), and the obtained images were processed using Affymetrix Microarray Suite version 5 (MAS5). MAS5 detection calls were calculated to examine the reliability of probe detection. The raw data obtained were analyzed using Bioconductor (Huber et al., 2015), and the signal values derived were globally normalized using guanine cytosine robust multiarray analysis (Wu and Irizarry, 2004).

2.3. MRI measurement

Marmosets ($n = 16$; Table 1) were sedated and euthanized as carried out for the microarray analysis. They were then intracardially perfused with 0.1 M PBS, followed by 4% paraformaldehyde (Merck, Whitehouse Station, NY, USA) in 0.1 M PBS. Fixed brain samples were placed into 50 mL polypropylene centrifuge tubes filled with 4% paraformaldehyde in PBS and supported by a handmade brain holder. The space between the coil and the measurement tube was filled with a piece of sponge to

Table 1
Summary of VPA and UE groups used in the microarray and DTI analyses.

Condition	Experiments	Age (days)	Body weight (g)	Sex
UE	Microarray	0	29	Male
UE	Microarray	1	32	Female
UE	Microarray	1	24	Female
UE	Microarray	4	24	Male
UE	DTI	2	26	Female
UE	DTI	2	30	Female
UE	DTI	2	26	Female
UE	DTI	2	32	Female
UE	DTI	2	28	Female
UE	DTI	2	22	Male
UE	DTI	2	28	Male
UE	DTI	2	24	Male
UE	DTI	2	22	Male
VPA	Microarray	0	30	Female
VPA	Microarray	0	25	Female
VPA	Microarray	0	30	Male
VPA	Microarray	1	30	Female
VPA	DTI	2	30	Female
VPA	DTI	2	30	Female
VPA	DTI	2	28	Female
VPA	DTI	2	30	Female
VPA	DTI	2	32	Male
VPA	DTI	2	32	Male
VPA	DTI	2	27	Male

VPA, valproic acid; UE, unexposed; DTI, diffusion tensor imaging.

suppress noise caused by vibration. The sample temperature was maintained at room temperature (23.0 °C ± 0.5 °C) during imaging. T1-, T2-, and diffusion-weighted images (DWI) of the *ex vivo* brain samples were obtained on a 7-Tesla, 20-cm-bore MRI (BioSpec AVANCE-III, Bruker Biospin, Ettlingen, Germany), with a volume resonator of 8.5-cm inner diameter for transmission and an 8-channel phased array coil for reception (Bruker Biospin). The data obtained were reconstructed using ParaVision 5.1 (Bruker Biospin).

For T2-weighted and diffusion tensor imaging (DTI), we used a two-dimensional (2D) spin-echo sequence with a motion probing gradient (DtiStandard, Bruker Biospin) according to the following parameters: repetition time (T_R) = 6500 ms; echo time (T_E) = 26.6 ms; field of view (FOV) = 32.0 × 32.0 mm^2; matrix size = 192 × 192; number of slices = 11; slice thickness = 1.0 mm; slice gap = 0; number of averages = 15; total scan time = 36 h 24 min. We obtained one set of T2-weighted images without the motion probing gradient as well as six sets of DWI with different diffusion directions (δ = 7 ms; Δ = 14 ms; *b*-value = 1000 s/mm^2).

T1-weighted images were obtained using the modified driven equilibrium Fourier transform sequence with the following parameters: T_R = 3000 ms; T_E = 4.2 ms; echo repetition time = 13.8 ms; number of segments = 8; inversion delay = 975 ms; FOV = 32.0 × 32.0 × 24.0 mm^3; matrix size = 256 × 256 × 96; number of averages = 14; total scan time = 8 h 57 min. We computed color-encoded orientation and fractional anisotropy (FA) maps using TracVis version 0.6.0.1 and Diffusion Toolkit version 0.6.3, a set of data reconstruction tools distributed by Wang and Van (Martinos Center, Massachusetts General Hospital, Boston, MA, USA). Two regions-of-interest, AC and CC, were detected at the midsagittal plane of the FA maps.

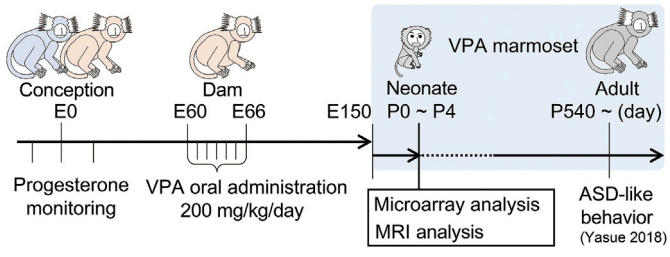

Fig. 1. Experimental schedule. The figure illustrates the experimental schedule for producing and analyzing VPA marmosets. VPA was administered *in utero* at E60-E66. For microarray and MRI analyses, brain samples of the VPA and UE groups were obtained at P0-P4. Note that the same VPA treatment has induced social cognition deficits in adulthood in previous studies (Yasue et al., 2015, 2018). VPA, valproic acid; UE, unexposed; E, Embryonic day; MRI, magnetic resonance imaging; P, postnatal day.

2.4. Histology

Myelin staining was performed in 40-μm-thick parasagittal sections taken from the neonatal marmosets. The sections were immersed in 0.005% Triton X-100 in 0.01 M PB for 30 min so that they remained attached to gelatin-coated glass slides throughout the staining protocol. Next, the sections were washed in 0.01 M PB, mounted on the glass slides, and dried overnight at 4 °C. Finally, they were stained for myelin in accordance with the protocol of Larsen et al. (2003).

2.5. Data analysis

For data analysis of gene expression, we used Matlab 2017b (Mathworks, Inc., Natick, MA, USA). We compared gene expression levels between the VPA and UE groups; we used genes where >50% of the MAS5 signal detection calls were Present-call (McClintick and Edenberg, 2006). If one gene symbol corresponded to multiple probes, we used the mean value of all corresponding probes as the gene expression value. The expression level for each gene symbol was compared between the VPA and UE groups using Welch's *t*-test. The *p*-values were then corrected using the Benjamini–Hochberg false discovery rate (BH-FDR) method (Benjamini and Hochberg, 1995). Genes with *p*-values <0.01 and more than 2-fold changes were selected for pathway analysis based on the Kyoto Encyclopedia of Genes and Genomes (KEGG) pathway database (Kanehisa and Goto, 2000).

Imaging data analysis was performed using the following series of semi-automatic procedures. (i) The FA maps were reconstructed into high spatial resolution images (pixel size 0.05 mm × 0.05 mm) using a beta-spline interpolation method. (ii) The edges of the midsagittal AC and CC areas were defined using the Canny edge detection algorithm (Gaussian filter parameter; σ = 0.75) (Canny, 1986; Pau et al., 2010). (iii) The whole brain (WB) sizes were circulated from T1-weighted MR images using the same edge detection algorithm, without interpolation. (iv) Statistical significance between the VPA and UE groups for size and FA values of AC and CC, and the WB size were calculated using the Brunner–Munzel test (BM test), a non-parametric studentized permutation test (Brunner and Munzel, 2000). All analyses were performed using R version 3.4.0 and its packages {biOps} version 0.2.1, {EBImage} version 4.12.2, and {lawstat} version 3.4.3.

3. Results

3.1. Downregulation of FZD3 and PIK3CA in the VPA group

We examined the influence of fetal VPA exposure on neonatal gene transcription using custom-made microarrays; we reliably detected transcript expression signals corresponding to 11,576 genes. Fig. 2A shows a scatter plot comparing the gene transcription level between the VPA and UE groups. No genes were significantly upregulated in the VPA group. However, we found 20 genes that exhibited significantly lower expression in the VPA group than in the UE group [red dots in Fig. 2A; BH-FDR-corrected *p*-value <0.01; fold change (FC) > 2]. These included one gene transcript (*FZD3*) downregulated more than 10-fold (FC = −11.63) and four gene transcripts (*CHRM3*, *ZKSCAN1*, *PIK3CA*, and *FAM76A*) downregulated about 4-fold in the VPA group (FC = −4.02, −4.00, −3.85, and −3.65, respectively) (Table 2).

We then performed KEGG pathway analysis (Kanehisa and Goto, 2000) using 20 differentially expressed genes. The analysis revealed that *FZD3* and *PIK3CA* appeared on the axon guidance pathway

(Wnt-FZD-PIK3 pathway; Fig. 2C). Accordingly, we compared the expression levels of *FZD3* and *PIK3CA* between the VPA and UE groups along with three well-known housekeeping genes — *LMNB1*, *GAPDH*, and *ACTB*. We found that the expression levels of *FZD3* and *PIK3CA* were consistently low in multiple VPA samples ($p < 0.001$), while those of *LMNB1*, *GAPDH*, and *ACTB* remained unchanged. Using Welch's *t*-test followed by Benjamini–Hochberg FDR multi-comparison correction, FCs in the expression levels of *LMNB1*, *GAPDH*, and *ACTB* between the VPA and UE groups were found to be −1.08, 1.05, and 1.27, respectively (BH-FDR-corrected *p*-value = 1.00, for each) (Fig. 2B).

Together, our comprehensive gene expression analysis revealed that two genes in the Wnt–FZD–PIK3 signaling pathway were largely downregulated in the VPA group. This signaling pathway mediates commissural axon attraction and proper anterior–posterior pathfinding (Salinas et al., 2008). Thus our results suggest that fetal VPA exposure may induce abnormalities of commissural axons, such as AC and CC.

3.2. Reduced AC size in the VPA group

Next, we examined structural abnormalities in AC and CC of VPA-exposed neonates using DTI. We obtained DTI data from 16 fixed brain samples at P2 (VPA: $n = 7$; UE: $n = 9$). As expected, both AC and CC were clearly visible on the midsagittal plane in the color-encoded orientation maps as high-diffusion areas along the left–right orientation (blue regions in Fig. 3); they were successfully delineated by the Canny edge detection algorithm on the midsagittal plane in the FA maps (Fig. 4A–C). We measured the size of each area (Fig. 4D) and then individually normalized it by the WB volume. The normalized AC area in the VPA group appeared significantly smaller than that in the UE group (Fig. 4E; median value: *p*-value = 0.041 with BM test, with BM statistic = −2.27; *df* = 12.77). By contrast, we observed no significant difference in the normalized CC areas (Fig. 4E; *p*-value = 0.62) or in WB sizes between the VPA and UE groups (Fig. 4F; *p*-value = 0.45 in the BM test). The between-group mean FA values in both AC and CC were not significantly different (Fig. 4G; AC: *p*-value = 0.53; CC: *p*-value = 0.96, both in the BM test). No individual marmoset provided outlier data for more than one parameter in the boxplots (Fig. 4E–G).

Finally, we performed myelin staining on sagittal sections in VPA and UE marmosets. AC and CC in both groups were identified as non-stained tissues, indicating that they were virtually nonmyelinated (Fig. 5, bottom), which was in agreement with previous studies in rhesus monkeys (LaMantia and Rakic, 1990, 1994). Despite careful processing, we were unable to precisely cut the brain at the midsagittal plane while restoring the shape of CC completely (Fig. 5, top), and therefore histological verification of the AC and CC sizes was not attempted. However, our results suggest that DTI images provide a useful means for measuring neonatal bilateral commissural structures.

4. Discussion

Many neuroimaging studies have reported disrupted functional and structural connectivity in the social brain of ASD patients. Because ASD is a neurodevelopmental disorder with early onset of symptoms, it is important to identify neurostructural abnormalities at birth that might be associated with social recognition deficits in later life. In this study, we examined the neonatal brains of a marmoset ASD model that was

Table 2
Summary of the genes significantly downregulated in the VPA group.

Gene symbol	FC	*p*-value	Short description
FZD3	−11.63	0.0000108	frizzled homolog 3 (Drosophila)
CHRM3	−4.02	0.00965	cholinergic receptor, muscarinic 3
ZKSCAN1	−4	0.000518	zinc finger with *KRAB* and *SCAN* domains 1
PIK3CA	−3.85	0.000816	phosphoinositide-3-kinase, catalytic, alpha polypeptide
FAM76A	−3.65	0.00151	family with sequence similarity 76, member A
RGS7BP	−3.43	0.00711	regulator of G-protein signaling 7 binding protein
FAM130A2	−3.4	0.00322	family with sequence similarity 130, member A2
CREB1	−3.33	0.00711	cAMP responsive element binding protein 1
ASAM	−3.05	0.00448	adipocyte-specific adhesion molecule
SYT14	−3.05	0.000816	synaptotagmin XIV
RFX3	−2.95	0.00715	regulatory factor X, 3 (influences HLA class II expression)
CCNT1	−2.89	0.00222	cyclin T1
ZNF566	−2.65	0.00923	zinc finger protein 566
DIMT1L	−2.52	0.0000889	DIM1 dimethyladenosine transferase 1-like (*S. cerevisiae*)
HOOK3	−2.42	0.00965	hook homolog 3 (Drosophila)
XK	−2.21	0.00119	X-linked Kx blood group (McLeod syndrome)
TSPAN5	−2.16	0.000974	tetraspanin 5
RCP9	−2.13	0.00812	calcitonin gene-related peptide-receptor component protein
CCDC75	−2.08	0.000668	coiled-coil domain containing 75
FAM69A	−2.04	0.00711	family with sequence similarity 69, member A

VPA, valproic acid

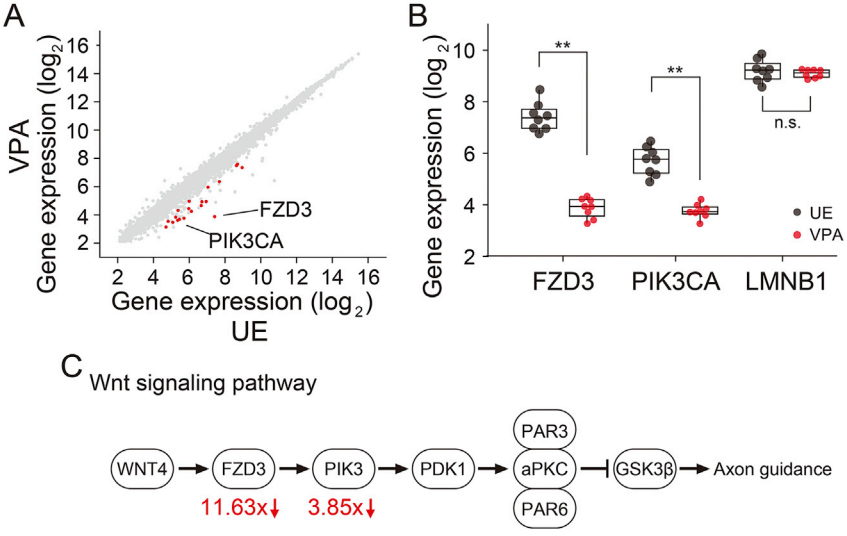

Fig. 2. Comparison of gene expression in VPA and UE neonatal marmosets. (A) Scatter plot comparing gene expression between the VPA and UE groups. The *x* and *y* axes indicate the mean intensity of gene expression in the UE and VPA groups, respectively. Red dots represent genes that were significantly downregulated ($p < 0.01$, BH-FDR corrected *p*-value) and had FCs >2. (B) Expression levels of *FZD3*, *PIK3CA*, and *LMNB1* (control housekeeping gene; similar results were obtained with other genes such as *GAPDH* and *ACTB*) in the VPA and UE groups. The boxplot represents the median and the first and third quartiles of the VPA (red) and UE groups (black) ($n = 8$ each; 4 subjects × 2 brain regions). ** $p < 0.001$ (significant difference); n.s., nonsignificant. (C) Illustration of the Wnt-FZD3-PIK3 signaling pathway. Arrows indicate positive regulation, whereas the line ending with a bar indicates negative regulation. The numbers below represent the mean times decrease in the gene expression observed in the VPA group. VPA, valproic acid; UE, unexposed; BH-FDR, Benjamini–Hochberg false discovery rate; FC, fold change

established to show social recognition deficits in adulthood. We demonstrated that fetal VPA exposure decreases the expression levels of two axon guidance related genes, *FZD3* and *PIK3CA*, in parts of the neonatal social brain (i.e., OFC and the inferior temporal cortex). DTI analysis demonstrated that VPA exposure *in utero* significantly decreases AC size, but not CC or WB size. In the following section, we first discuss the technical considerations for DTI analysis, both the advantages and limitations. We then discuss the relevance of these genetic and neurostructural signatures in neonatal marmosets with regard to findings of previous studies on human neuroimaging and rodent ASD models, and suggest the linkages to social cognitive dysfunction seen in adulthood.

4.1. Technical considerations, advantages, and limitations

The current study focused on the VPA-induced neurostructural abnormalities in AC and CC, the two major commissures connecting the bilateral social brain. For this purpose, we performed DTI measurement on fixed neonatal brain samples, visualizing macroscopic axonal organizations in neural tissues by referring to water anisotropic diffusion. We found that the midsagittal AC areas, identified as high-diffusion areas, were significantly decreased in VPA marmosets, while the mean FA values were unchanged. In general, white matter FA values are regarded as reflecting many factors including axonal counts and density, degree of myelination, and fiber organization (Jelescu and Budde, 2017). Since AC and CC were not yet myelinated at this early postnatal stage (cf. Fig. 5), the AC area reduction in the VPA group may reflect abnormal axonal development, presumably consisting of a decrease in the number of AC axons.

Histological analysis using myelin staining provided information regarding axonal maturation with fine resolution. However, it fails to provide a quantitative measurement of nanostructures on the midsagittal plane because of inevitable nonlinear distortion of brain sections due to the staining process. In contrast, DTI offers visualization of the midsagittal plane by simply adjusting the position and the angle of slices to the brain sample in the console. Because the axon bundles at birth are immature and not yet myelinated, we optimized the DTI sequence and the sample conditions in order to enhance the weak diffusion signals. Our original magnetic resonance sequence for a 7-Tesla scanner provided diffusion weights with high spatial resolution (anterior–posterior and dorsal–ventral axes, 166 μm/pixel; Fig. 3), which enabled us to qualify the microstructures on the midsagittal plane. Our image–processing pipeline, in combination with the Canny edge detection algorithm and beta-spline interpolation, reliably detected both AC and CC, and thereby performing segmentation automatically. We did not use contrast agents like Fomblin (Liu et al., 2018; Sati et al., 2012), because their effects on histological staining have not been fully examined. We measured fixed brains in nonisometric voxels (resolution of left–right axis, 1 mm) for a long total scan time (~45 h). Because of this limitation, we could not extend our analysis to 3D tractography to examine other structural connectivities, including hippocampal and habenular commissures. While the DTI methodology needs to be improved in terms of signal-to-noise ratio and scan time, *in vivo* longitudinal measurements of structural connectivity are an attractive challenge for further analysis of this marmoset model.

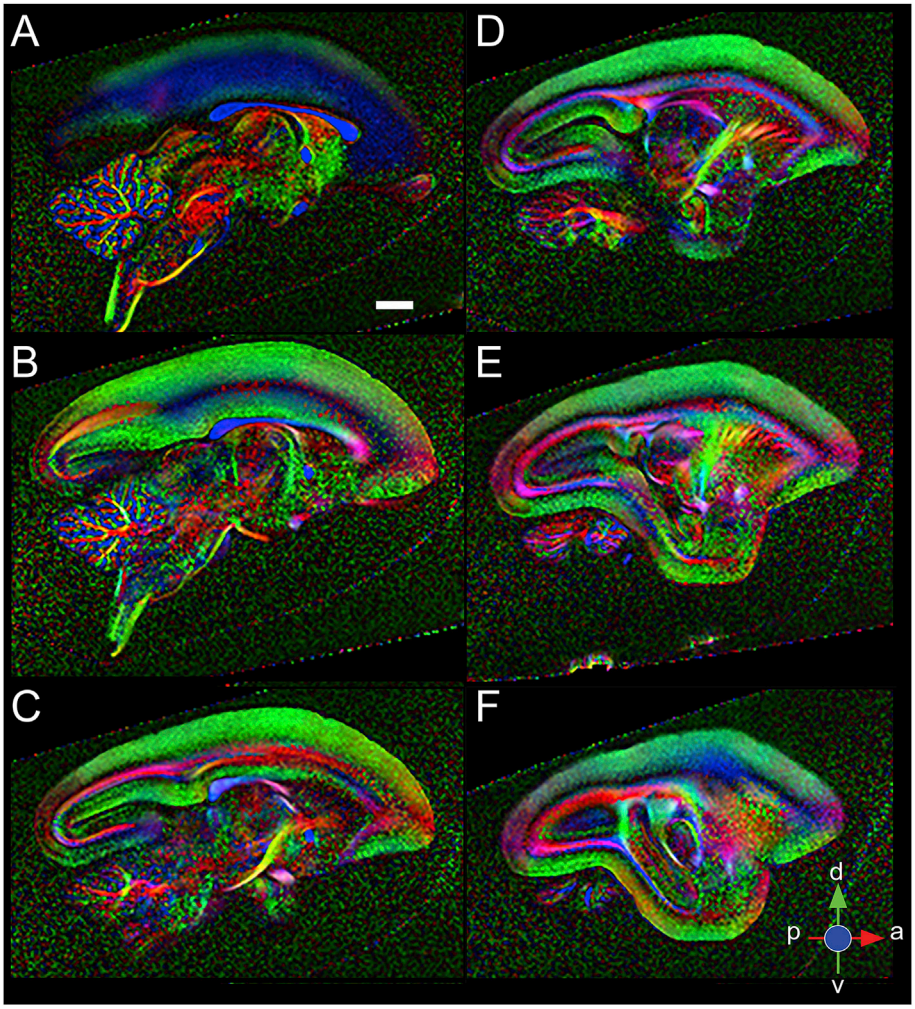

Fig. 3. AC and CC structures in DTI color-encoded orientation maps of a neonatal marmoset brain. AC (white arrowheads) and CC (yellow arrowheads) were clearly visualized in sagittal slices of diffusion tensor images at P2 in the common marmoset. Figures represent the data from the midsagittal plane (A) to the left side (F) in 1-mm-thick slices. Red, green, and blue colors encode the orientation of maximal diffusion along the anterior–posterior, dorsal–ventral, and left–right directions, respectively. Scale bar = 3 mm. AC, anterior commissure; CC, corpus callosum; DTI, diffusion tensor imaging; P, postnatal day

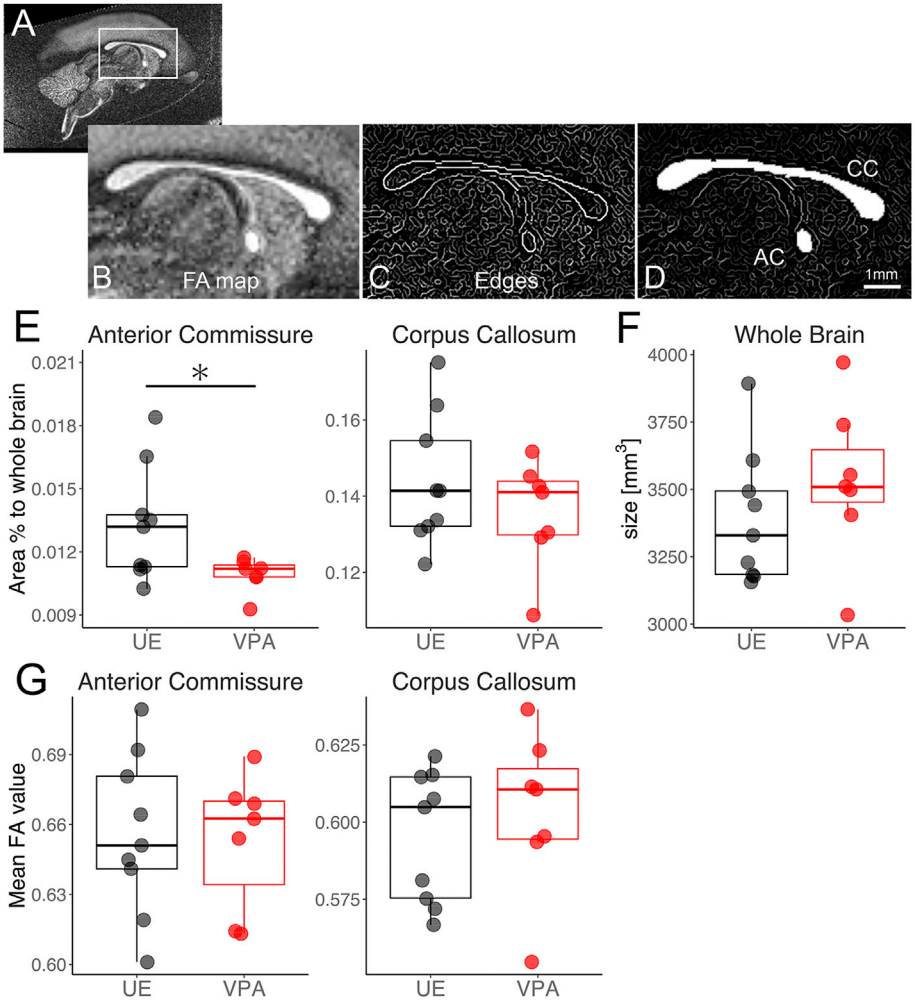

Fig. 4. Comparisons of AC and CC sizes in VPA and UE neonatal marmosets. (A) Representative FA map in the midsagittal plane. (B) Enlarged view of the boxed region in (A). (C, D) Delineation of AC and CC areas using the Canny edge detection algorithm. (E) Comparison of AC and CC sizes between the UE (black, $n = 9$) and VPA groups (red, $n = 7$). AC and CC areas were normalized individually by the WB size. The AC size in the VPA group was significantly smaller than that in the UE group ($p < 0.05$ in BM test for median value). (F) Between-group comparison of the WB size. (G) Between-group comparison of mean FA values for AC and CC. AC, anterior commissure; CC, corpus callosum; VPA, valproic acid; UE, unexposed; FA, fractional anisotropy; BM, Brunner–Munzel; WB, whole brain

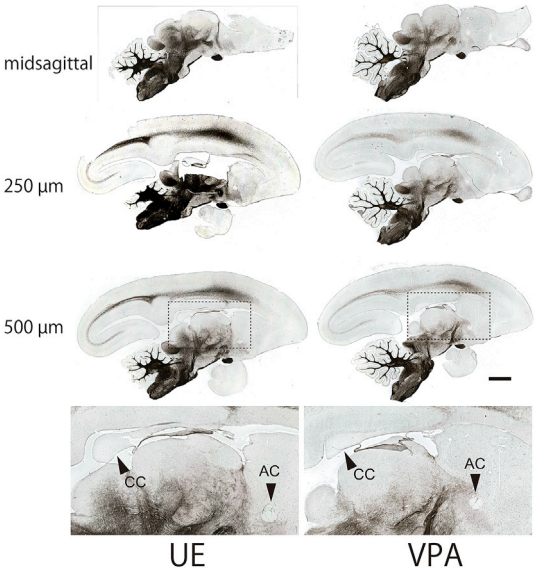

Fig. 5. Sagittal sections of myelin staining of UE and VPA neonatal marmoset brains. Representative low-magnification images of WB sections 0, 250, and 500 μm lateral from the midsagittal plane are shown from top to third row, while high-magnification images focusing on the AC and CC areas are shown in the bottom row. Scale bar = 1 mm. UE, unexposed; VPA, valproic acid; WB, whole brain; AC, anterior commissure; CC, corpus callosum

4.2. *VPA-induced genetic alterations associated with immature axonal growth at birth*

Fetal VPA exposure is a well-known risk factor for ASD in humans (Christensen et al., 2013), and it is one of the most widely used models of ASD (Roullet et al., 2013). Studies on rodent models have suggested that rat pups exhibiting social interaction deficits in adulthood are produced from dams exclusively treated with VPA at around embryonic day (E)12, corresponding to neural tube closure (Kataoka et al., 2013; Kim et al., 2011). VPA is a histone deacetylase inhibitor, meaning that it induces broad and complex epigenetic alterations in exposed embryonic brain, including abnormal processing on the axon guidance signaling proteins ERK1/2 and PKC as well as canonical Wnt signaling proteins such as GSK-3β (Go et al., 2012; Cohen et al., 2013). VPA exposure in E12.5 rats also promotes neurite overgrowth and axonal over-regeneration in the fetal brain (Zhang et al., 2018). However, the genetic mechanism that links fetal VPA exposure and social brain pathologies underlying social communication and interaction disabilities in adults remains unknown.

The marmoset VPA model used in this study, which consisted of dams who were administered VPA on E60–E66 (Carnegie stage 11–15, corresponding to the developmental stage of E12.5 rats; see Butler and Juurlink, 2018), has demonstrated social recognition deficits in adulthood (Yasue et al., 2015, 2018). The comprehensive gene expression analysis of this study identified two genes on the axon guidance signaling pathway, *FZD3* and *PIK3CA*, which were largely downregulated in the social brain of the neonatal VPA group. The Wnt–FZD–PIK3 signaling pathway mediates commissural axon attraction and proper

anterior–posterior pathfinding (Salinas et al., 2008). Studies on *FZD3*-mutant mice have reported axonal growth deficits, such as misdirection of commissural axons along the anterior–posterior axis and a loss, or at least a significant reduction, of the main long-distance axons, including AC and CC (Wolf et al., 2018; Wang et al., 2002, 2006; Hue et al., 2014).

The current study also demonstrated that the size of AC, but not that of CC, significantly decreases in VPA marmosets. Why is the AC pathway specifically affected by the VPA treatment? One possibility is that the VPA administration may affect the different stages in axonal growth of AC and CC. Indeed, in the human embryo, AC begins to cross the midline at E9–10 week, while CC begins to traverse the midline at E11–12 week (Rakic and Yakovlev, 1968). Thus, fetal VPA exposure in primates may alter *Wnt–FZD3–PIK3* signaling, leading to abnormal processing in axonal growth and commissural guidance of AC specifically. The reduced AC size in our VPA-exposed neonates at birth, therefore, might reflect abnormal development or guidance of the axonal bundle.

4.3. Reduced AC size as a neurostructural abnormality signature leading to social brain dysfunction

Adaptive social behavior, efficient social recognition, and communication all require rapid implementation of multiple high-order functions such as face recognition, vocal communication, body motion recognition, internal state estimation, and decision making (Adolphs, 2001). Hence, social cognitive abilities depend on computations via distributed networks that connect the social brain (Wang and Olson, 2018). Social cognitive skill impairment in ASD patients is probably due to a decrease in the interhemispheric connections of the social brain responsible for higher-order associations. This hypothesis is supported by functional imaging studies on humans that demonstrate weak functional connectivity across the two brain hemispheres in ASD patients as well as in at-risk infants (Geschwind and Levitt, 2007; Wolff et al., 2015; Frazier and Hardan, 2009; Dinstein et al., 2011). AC bilaterally connects the two brain hemispheres, specifically the regions constituting a large part of the social brain: OFC, temporal pole, temporal lobe including rostral superior temporal region, superior temporal sulcus region, and amygdala (Amaral et al., 2008; Brothers, 2002; Schmahmann and Pandya, 2006). In primates, AC is a relatively small axonal bundle compared with CC (percentage of CC size: humans, ~1%; macaques, ~5%; common marmosets, ~8%) (Foxman et al., 1986; this study). However, previous studies on AC and CC lesions in monkeys have already suggested the relatively large contribution of AC to interhemispheric processing; AC is responsible for interhemispheric transfer of visual memory in monkeys (Sullivan, 1973). It has also been shown that AC and CC lesions severely reduce interhemispheric functional connectivity, but this effect is greatly mitigated if AC is left intact (O'Reilly et al., 2013). In spite of the importance of AC for interhemispheric functional connectivity in the social brain in primates, AC has received little attention in the research on structural abnormality in ASD patients.

As discussed in the previous section, our finding, reduced AC size of VPA-exposed neonates at birth, might reflect abnormal growth or guidance of the axonal bundle connecting a large part of the social brain. We speculate that the reduction of bilateral anatomical connection at birth may hamper the normal development of interhemispheric organization of both cortico-cortical and cortico-subcortical structures, resulting in social cognitive dysfunctions in later life. In fact, recent neuroimaging study has demonstrated that, by 6 months of age, high-risk infants who are classified as ASD later already display deficiencies in corticocortical organization (Lewis et al., 2017), indicating that the neuropathology of ASD surely arises at an earlier stage of life.

By contrast, fetal VPA exposure did not change the size of CC in marmosets at birth. This might contradict the common view of structural abnormalities in ASD patients, that is, a decreased mean CC size (Frazier and Hardan, 2009). However, recent imaging studies have suggested that the size of CC could, in fact, increase in ASD infants (6–24 months old) (Wolff et al., 2015; Travers et al., 2015); thus, it remains unclear just when the atypical CC morphology of ASD first emerges. CC comprises topographically organized microstructures (Schmahmann and Pandya, 2006), and partial structural alterations within CC have also been specified in ASD patients (Wolff et al., 2015). In the current study, however, because of limited DTI resolution, partial CC sizes were not investigated; future studies are required to assess the substructual abnormalities of CC in this model.

In summary, the current findings—reduced AC size and axon guidance signaling in VPA marmosets—may provide a novel risk factor of ASD for weakening interhemispheric connections at birth, hampering normal development of social brain function. Although a clear mechanistic link remains missing, our results highlight the importance of future research efforts in investigating the neuropathology of VPA model marmosets, as well as neuroimaging analysis focusing on AC.

5. Conclusion

In this study, we demonstrated that fetal VPA exposure decreases the expression of axon guidance signaling pathway genes in parts of the social brain of neonatal marmosets. This finding is consistent with previous rodent models and highlights the critical contribution of *Wnt–FZD3–PIK3* signaling to abnormal axon growth or guidance in the neonatal primate brain. We also found a significant AC size reduction in the neonatal marmoset VPA model. Since AC bilaterally connects the two brain hemispheres, specifically the regions constituting the social brain (e.g., OFC and inferior temporal cortex), a diminishment of this axonal connection in neonatal primates might be a critical neurostructural risk factor hampering the development of normal social brain function. Although the literature concerning ASD has focused little on AC, the findings of this study might provide novel genetic and neurostructural signatures at birth that could represent potential targets for early intervention.

Authors' contributions

KM and NI planned the experiment. KN prepared the VPA marmoset group. TO and TS sampled brain parts for the gene chip analysis. TO, KSumida, KSaito, KH, and IM analyzed the gene chip data. MK fixed brains for MRI imaging. IA, CS, KM, and TS performed the MRI imaging. KM, TO, AI, TM, and NI wrote the manuscript. All authors were involved in the preparation of the manuscript. All authors read and approved the final manuscript.

Conflicts of interest

The authors declare no conflicts of interest for this study.

Funding

This research was supported by an Intramural Research Grant (grant number 23–7) for Neurological and Psychiatric Disorders from the National Center of Neurology and Psychiatry; by a Funding Program for World-Leading Innovative R&D on Science and Technology (FIRST Program); by MEXT KAKENHI [JP25110740, JP25117001 (to NI), JP26118717 (to NI), and JP17H06040 (to KM)]; and by AMED [JP18dm0207001 (to NI), JP16cm0106202 (to IA), JP17dm0107066 (to IA), JP18dm0207007 (to TS), and JP18dm0307007 (to TM)]. This research was partly supported by a COI program by JST (to IA).

Acknowledgments

We thank Mr. Nobuhiro Nitta for his excellent technical assistance with MRI, Ms. Tomoko Manabe for her wonderful technical assistance with histology, and Mr. Hajime Ishii for his valuable technical support and animal care.

References

Adolphs, R., 2001. The neurobiology of social cognition. Curr. Opin. Neurobiol. 11, 231–239. https://doi.org/10.1016/S0959-4388(00)00202-6.

Amaral, D.G., Schumann, C.M., Nordahl, C.W., 2008. Neuroanatomy of autism. Trends Neurosci. 31, 137–145. https://doi.org/10.1016/j.tins.2007.12.005.

Benjamini, Y., Hochberg, Y., 1995. Controlling the false discovery rate: a practical and powerful approach to multiple testing. J. R. Stat. Soc. Ser. B 57, 289–300.

Brothers, L., 2002. The social brain: a project for integrating primate behavior and neurophysiology in a new domain. In: Cacioppo, J.T. (Ed.), Foundations in Social Neuroscience. MIT Press, Cambridge, pp. 367–385. https://doi.org/10.1093/schbul/sbq012.

Brunner, E., Munzel, U., 2000. The nonparametric behrens-Fisher problem: asymptotic theory and a small-sample approximation. Biom. J. 42, 17–25.

Burkart, J.M., Fehr, E., Efferson, C., van Schaik, C.P., 2007. Other-regarding preferences in a non-human primate: common marmosets provision food altruistically. Proc. Natl. Acad. Sci. U. S. A. 104, 19762–19766. https://doi.org/10.1073/pnas.0710310104.

Burman, K.J., Rosa, M.G., 2009. Architectural subdivisions of medial and orbital frontal cortices in the marmoset monkey (Callithrix jacchus). J. Comp. Neurol. 514, 11–29. https://doi.org/10.1002/cne.21976.

Butler, H., Juurlink, B.H.J., 2018. An Atlas for Staging Mammalian and Chick Embryos. CRC Press, Place of publication not identified, p. 1 online resource (232 pages).

Canny, J., 1986. A computational approach to edge detection. IEEE Trans. Pattern Anal. Mach. Intell. 8, 679–698. https://doi.org/10.1109/TPAMI.1986.4767851.

Christensen, J., Gronborg, T.K., Sorensen, M.J., Schendel, D., Parner, E.T., Pedersen, L.H., Vestergaard, M., 2013. Prenatal valproate exposure and risk of autism spectrum disorders and childhood autism. J. Am. Med. Assoc. 309, 1696–1703. https://doi.org/10.1001/jama.2013.2270.

Cohen, O.S., Varlinskaya, E.I., Wilson, C.A., Glatt, S.J., Mooney, S.M., 2013. Acute prenatal exposure to a moderate dose of valproic acid increases social behavior and alters gene expression in rats. Int. J. Dev. Neurosci. 31, 740–750. https://doi.org/10.1016/j.ijdevneu.2013.09.002.

Di Martino, A., Ross, K., Uddin, L.Q., Sklar, A.B., Castellanos, F.X., Milham, M.P., 2009. Functional brain correlates of social and nonsocial processes in autism spectrum disorders: an activation likelihood estimation meta-analysis. Biol. Psychiatry 65, 63–74. https://doi.org/10.1016/j.biopsych.2008.09.022.

Dinstein, I., Pierce, K., Eyler, L., Solso, S., Malach, R., Behrmann, M., Courchesne, E., 2011. Disrupted neural synchronization in toddlers with autism. Neuron 70, 1218–1225. https://doi.org/10.1016/j.neuron.2011.04.018.

Foxman, B.T., Oppenheim, J., Petito, C.K., Gazzaniga, M.S., 1986. Proportional anterior commissure area in humans and monkeys. Neurology 36, 1513–1517. https://doi.org/10.1212/WNL.36.11.1513.

Frazier, T.W., Hardan, A.Y., 2009. A meta-analysis of the corpus callosum in autism. Biol. Psychiatry 66, 935–941. https://doi.org/10.1016/j.biopsych.2009.07.022.

Frith, U., Morton, J., Leslie, A.M., 1991. The cognitive basis of a biological disorder: autism. Trends Neurosci. 14, 433–438.

Gallagher, H.L., Frith, C.D., 2003. Functional imaging of 'theory of mind. Trends Cognit. Sci. 7, 77–83. https://doi.org/10.1016/S1364-6613(02)00025-6.

Geschwind, D.H., Levitt, P., 2007. Autism spectrum disorders: developmental disconnection syndromes. Curr. Opin. Neurobiol. 17, 103–111. https://doi.org/10.1016/j.conb.2007.01.009.

Go, H.S., Kim, K.C., Choi, C.S., Jeon, S.J., Kwon, K.J., Han, S.H., Lee, J., Cheong, J.H., Ryu, J.H., Kim, C.H., Ko, K.H., Shin, C.Y., 2012. Prenatal exposure to valproic acid increases the neural progenitor cell pool and induces macrocephaly in rat brain via a mechanism involving the GSK-3beta/beta-catenin pathway. Neuropharmacology 63, 1028–1041. https://doi.org/10.1016/j.neuropharm.2012.07.028.

Hazlett, H.C., Gu, H., Munsell, B.C., Kim, S.H., Styner, M., Wolff, J.J., Elison, J.T., Swanson, M.R., Zhu, H., Botteron, K.N., Collins, D.L., Constantino, J.N., Dager, S.R., Estes, A.M., Evans, A.C., Fonov, V.S., Gerig, G., Kostopoulos, P., McKinstry, R.C., Pandey, J., Paterson, S., Pruett, J.R., Schultz, R.T., Shaw, D.W., Zwaigenbaum, L., Piven, J., the IBIS Network, 2017. Early brain development in infants at high risk for autism spectrum disorder. Nature 542, 348–351. https://doi.org/10.1038/nature21369.

Herve, P.Y., Razafimandimby, A., Vigneau, M., Mazoyer, B., Tzourio-Mazoyer, N., 2012. Disentangling the brain networks supporting affective speech comprehension. Neuroimage 61, 1255–1267. https://doi.org/10.1016/j.neuroimage.2012.03.073.

Hua, Z.L., Jeon, S., Caterina, M.J., Nathans, J., 2014. Frizzled3 is required for the development of multiple axon tracts in the mouse central nervous system. Proc. Natl. Acad. Sci. U. S. A. 111, E3005–E3014. https://doi.org/10.1073/pnas.1406399111.

Huber, W., Carey, V.J., Gentleman, R., Anders, S., Carlson, M., Carvalho, B.S., Bravo, H.C., Davis, S., Gatto, L., Girke, T., Gottardo, R., Hahne, F., Hansen, K.D., Irizarry, R.A., Lawrence, M., Love, M.I., MacDonald, J., Obenchain, V., Oles, A.K., Pages, H., Reyes, A., Shannon, P., Smyth, G.K., Tenenbaum, D., Waldron, L., Morgan, M., 2015. Orchestrating high-throughput genomic analysis with Bioconductor. Nat. Methods 12, 115–121. https://doi.org/10.1038/nmeth.3252.

Jelescu, I.O., Budde, M.D., 2017. Design and validation of diffusion MRI models of white matter. Frontiers in physics 5, 61. https://doi.org/10.3389/fphy.2017.00061.

Kanehisa, M., Goto, S., 2000. KEGG: kyoto encyclopedia of genes and genomes. Nucleic Acids Res. 28, 27–30. https://doi.org/10.1093/nar/28.1.27.

Kataoka, S., Takuma, K., Hara, Y., Maeda, Y., Ago, Y., Matsuda, T., 2013. Autism-like behaviours with transient histone hyperacetylation in mice treated prenatally with valproic acid. Int. J. Neuropsychopharmacol. 16, 91–103. https://doi.org/10.1017/S1461145711001714.

Kawai, N., Yasue, M., Banno, T., Ichinohe, N., 2014. Marmoset monkeys evaluate third-party reciprocity. Biol. Lett. 10, 20140058-20140058. https://doi.org/10.1098/rsbl.2014.0058.

Kim, K.C., Kim, P., Go, H.S., Choi, C.S., Yang, S.I., Cheong, J.H., Shin, C.Y., Ko, K.H., 2011. The critical period of valproate exposure to induce autistic symptoms in Sprague-Dawley rats. Toxicol. Lett. 201, 137–142. https://doi.org/10.1016/j.toxlet.2010.12.018.

LaMantia, A.S., Rakic, P., 1990. Axon overproduction and elimination in the corpus callosum of the developing rhesus monkey. J. Neurosci. 10, 2156–2175.

LaMantia, A.S., Rakic, P., 1994. Axon overproduction and elimination in the anterior commissure of the developing rhesus monkey. J. Comp. Neurol. 340, 328–336. https://doi.org/10.1002/cne.903400304.

Larsen, M., Bjarkam, C.R., Stoltenberg, M., Sorensen, J.C., Danscher, G., 2003. An autometallographic technique for myelin staining in formaldehyde-fixed tissue. Histol. Histopathol. 18, 1125–1130. https://doi.org/10.14670/HH-18.1125.

Lewis, J.D., Evans, A.C., Pruett Jr., J.R., Botteron, K.N., McKinstry, R.C., Zwaigenbaum, L., Gerig, G., 2017. The emergence of network inefficiencies in infants with autism spectrum disorder. Biol. Psychiatry 82, 176–185. https://doi.org/10.1016/j.biopsych.2017.03.006.

Liu, C., Ye, F.Q., Yen, C.C., Newman, J.D., Glen, D., Leopold, D.A., Silva, A.C., 2018. A digital 3D atlas of the marmoset brain based on multi-modal MRI. Neuroimage 169, 106–116. https://doi.org/10.1016/j.neuroimage.2017.12.004.

McClintick, J.N., Edenberg, H.J., 2006. Effects of filtering by Present call on analysis of microarray experiments. BMC Bioinf. 7, 49. https://doi.org/10.1186/1471-2105-7-49.

Nelson, E.E., Winslow, J.T., 2008. Non-human primates: model animals for developmental psychopathology. Neuropsychopharmacology 34, 90–105. https://doi.org/10.1038/npp.2008.150.

O'Reilly, J.X., Croxson, P.L., Jbabdi, S., Sallet, J., Noonan, M.P., Mars, R.B., Browning, P.G., Wilson, C.R., Mitchell, A.S., Miller, K.L., Rushworth, M.F., Baxter, M.G., 2013. Causal effect of disconnection lesions on interhemispheric functional connectivity in rhesus monkeys. Proc. Natl. Acad. Sci. U. S. A. 110, 13982–13987. https://doi.org/10.1073/pnas.1305062110.

Oga, T., Aoi, H., Sasaki, T., Fujita, I., Ichinohe, N., 2013. Postnatal development of layer III pyramidal cells in the primary visual, inferior temporal, and prefrontal cortices of the marmoset. Front. Neural Circuits 7, 31. https://doi.org/10.3389/fncir.2013.00031.

Pau, G., Fuchs, F., Sklyar, O., Boutros, M., Huber, W., 2010. EBImage–an R package for image processing with applications to cellular phenotypes. Bioinformatics 26, 979–981. https://doi.org/10.1093/bioinformatics/btq046.

Pelphrey, K.A., Shultz, S., Hudac, C.M., Vander Wyk, B.C., 2011. Research review: constraining heterogeneity: the social brain and its development in autism spectrum disorder. JCPP (J. Child Psychol. Psychiatry) 52, 631–644. https://doi.org/10.1111/j.1469-7610.2010.02349.x.

Rakic, P., Yakovlev, P.I., 1968. Development of the corpus callosum and cavum septi in man. J. Comp. Neurol. 132, 45–72. https://doi.org/10.1002/cne.901320103.

Robins, D.L., 2008. Screening for autism spectrum disorders in primary care settings. Autism 12, 537–556. https://doi.org/10.1177/1362361308094502.

Ross, L.A., Olson, I.R., 2010. Social cognition and the anterior temporal lobes. Neuroimage 49, 3452–3462. https://doi.org/10.1016/j.neuroimage.2009.11.012.

Roullet, F.I., Lai, J.K., Foster, J.A., 2013. In utero exposure to valproic acid and autism–a current review of clinical and animal studies. Neurotoxicol. Teratol. 36, 47–56. https://doi.org/10.1016/j.ntt.2013.01.004.

Salinas, P.C., Zou, Y., 2008. Wnt signaling in neural circuit assembly. Annu. Rev. Neurosci. 31, 339–358. https://doi.org/10.1146/annurev.neuro.31.060407.125649.

Sasaki, T., Oga, T., Nakagaki, K., Sakai, K., Sumida, K., Hoshino, K., Miyawaki, I., Saito, K., Suto, F., Ichinohe, N., 2014a. Developmental expression profiles of axon guidance signaling and the immune system in the marmoset cortex: potential molecular mechanisms of pruning of dendritic spines during primate synapse formation in late infancy and prepuberty (I). Biochem. Biophys. Res. Commun. 444, 302–306. https://doi.org/10.1016/j.bbrc.2014.01.024.

Sasaki, T., Oga, T., Nakagaki, K., Sakai, K., Sumida, K., Hoshino, K., Miyawaki, I., Saito, K., Suto, F., Ichinohe, N., 2014b. Developmental genetic profiles of glutamate receptor system, neuromodulator system, protector of normal tissue and mitochondria, and reelin in marmoset cortex: potential molecular mechanisms of pruning phase of spines in primate synaptic formation process during the end of infancy and prepuberty (II). Biochem. Biophys. Res. Commun. 444, 307–310. https://doi.org/10.1016/j.bbrc.2014.01.023.

Sati, P., Silva, A.C., van Gelderen, P., Gaitan, M.I., Wohler, J.E., Jacobson, S., Reich, D.S., 2012. In vivo quantification of T2 anisotropy in white matter fibers in marmoset monkeys. Neuroimage 59, 979–985. https://doi.org/10.1016/j.neuroimage.2011.08.064.

Schmahmann, J.D., Pandya, D.N., 2006. Fiber Pathways of the Brain. Oxford University Press, Oxford; New York.

Sullivan, M.V., Hamilton, C.R., 1973. Memory establishment via the anterior commissure of monkeys. Physiol. Behav. 11, 873–879. https://doi.org/10.1016/0031-9384(73)90283-7.

Travers, B.G., Tromp do, P.M., Adluru, N., Lange, N., Destiche, D., Ennis, C., Nielsen, J.A., Froehlich, A.L., Prigge, M.B., Fletcher, P.T., Anderson, J.S., Zielinski, B.A., Bigler, E.D., Lainhart, J.E., Alexander, A.L., 2015. Atypical development of white matter microstructure of the corpus callosum in males with autism: a longitudinal investigation. Mol. Autism. 6, 15. https://doi.org/10.1186/s13229-015-0001-8.

Vivanti, G., Dissanayake, C., Victorian, A.T., 2016. Outcome for children receiving the early start denver model before and after 48 months. J. Autism Dev. Disord. 46, 2441–2449. https://doi.org/10.1007/s10803-016-2777-6.

Wang, Y., Olson, I.R., 2018. The original social network: white matter and social cognition. Trends Cognit. Sci. 22, 504–516. https://doi.org/10.1016/j.tics.2018.03.005.

Wang, Y., Thekdi, N., Smallwood, P.M., Macke, J.P., Nathans, J., 2002. Frizzled-3 is required for the development of major fiber tracts in the rostral CNS. J. Neurosci. 22, 8563–8573. https://doi.org/10.1523/JNEUROSCI.22-19-08563.2002.

Wang, Y., Zhang, J., Mori, S., Nathans, J., 2006. Axonal growth and guidance defects in Frizzled3 knock-out mice: a comparison of diffusion tensor magnetic resonance imaging, neurofilament staining, and genetically directed cell labeling. J. Neurosci. 26, 355–364. https://doi.org/10.1523/JNEUROSCI.3221-05.2006.

Wass, S., 2011. Distortions and disconnections: disrupted brain connectivity in autism. Brain Cogn. 75, 18–28. https://doi.org/10.1016/j.bandc.2010.10.005.

Wicker, B., Fonlupt, P., Hubert, B., Tardif, C., Gepner, B., Deruelle, C., 2008. Abnormal cerebral effective connectivity during explicit emotional processing in adults with autism spectrum disorder. Soc. Cogn. Affect. Neurosci 2008, 135–143. https://doi.org/10.1093/scan/nsn007.

Wolff, J.J., Gerig, G., Lewis, J.D., Soda, T., Styner, M.A., Vachet, C., Botteron, K.N., Elison, J.T., Dager, S.R., Estes, A.M., Hazlett, H.C., Schultz, R.T., Zwaigenbaum, L., Piven, J., Network, I., 2015. Altered corpus callosum morphology associated with autism over the first 2 years of life. Brain 138, 2046–2058. https://doi.org/10.1093/brain/awv118.

Wu, Z., Irizarry, R.A., 2004. Preprocessing of oligonucleotide array data. Nat. Biotechnol. 22, 656–658 author reply 658. https://doi.org/10.1038/nbt0604-656b.

Yamazaki, Y., Watanabe, S., 2009. Marmosets as a next-generation model of comparative cognition, Jpn. Psychol. Res. 51, 182–196. https://doi.org/10.1111/j.1468-5884.2009.00398.x.

Yasue, M., Nakagami, A., Banno, T., Nakagaki, K., Ichinohe, N., Kawai, N., 2015. Indifference of marmosets with prenatal valproate exposure to third-party non-reciprocal interactions with otherwise avoided non-reciprocal individuals. Behav. Brain Res. 292, 323–326. https://doi.org/10.1016/j.bbr.2015.06.006.

Yasue, M., Nakagami, A., Nakagaki, K., Ichinohe, N., Kawai, N., 2018. Inequity aversion is observed in common marmosets but not in marmoset models of autism induced by prenatal exposure to valproic acid. Behav. Brain Res. 343, 36–40. https://doi.org/10.1016/j.bbr.2018.01.013.

Zhang, R., Zhou, J., Ren, J., Sun, S., Di, Y., Wang, H., An, X., Zhang, K., Zhang, J., Qian, Z., Shi, M., Qiao, Y., Ren, W., Tian, Y., 2018. Transcriptional and splicing dysregulation in the prefrontal cortex in valproic acid rat model of autism. Reprod. Toxicol. 77, 53–61. https://doi.org/10.1016/j.reprotox.2018.01.008.

Zhao, H., Jiang, Y.H., Zhang, Y.Q., 2018. Modeling autism in non-human primates: opportunities and challenges. Autism Res. 11, 686–694. https://doi.org/10.1002/aur.1945.